Experimental and Theoretical Investigation of Hydrodynamic Drag Loads on Flexible Side-by-Side Blades

Zhilong Wei[1,2,*], Trygve Kristiansen[2], David Kristiansen[2], Yanlin Shao[1]
[1]Technical University of Denmark, Kgs. Lyngby, 2800, Denmark
[2]Norwegian University of Science and Technology, Trondheim, 7491, Norway
*zhilwei@dtu.dk

1 INTRODUCTION

Our recent experimental investigations of flexible side-by-side blades under both steady and unsteady flows have observed flutter in both scenarios. Flutter significantly impacts blade kinematics and the hydrodynamic drag experienced by the blades. Our numerical approach [1], utilizing the reactive force model, successfully reproduces flutter phenomena. In contrast, the traditional Morison's equation fails to trigger flutter. In the static regime where flutter does not occur, the bulk drag coefficients calibrated from experiments in steady and unsteady flows can be unified through an effective Cauchy number, allowing for the use of analytical models developed for steady flows in unsteady flows. In the flutter regime, using the bulk drag coefficient from steady flows underestimates the drag load in oscillatory flow.

2 THEORY

We start by considering a flexible blade with constant length l, width b, and thickness d, clamped at one end and initially oriented perpendicular to a uniform, steady flow U_c of fluid with density ρ. The system is governed by four non-dimensional parameters:

$$\beta = \frac{m_a}{\mu + m_a}, \mathrm{Ca^c} = \frac{1}{2}\frac{\rho C_D b U_c^2 l^3}{EI}, \mathrm{B} = \frac{(\rho_s - \rho) g b d l^3}{EI}, \text{ and } \lambda = \frac{2}{\pi}\frac{C_D}{C_M}\frac{l}{b}, \tag{1}$$

where ρ_s and EI are the structure density and bending stiffness, C_D and C_M are the cross-flow drag coefficient and added mass coefficient, respectively. Physically, the mass ratio β represents the proportion of fluid inertia relative to the total inertia of the system. The Cauchy number $\mathrm{Ca^c}$ quantifies the ratio of the drag force to the restoring force due to bending stiffness. The buoyancy parameter B indicates the ratio of the restoring force due to buoyancy (or weight if gravity force dominates) to that due to bending stiffness. The slenderness parameter λ is proportional to the length-to-width ratio l/b. In scenarios involving a uniform oscillatory flow $U(t) = \omega A \sin(\omega t)$, where A and ω are the amplitude and angular frequency of the oscillatory flow, an additional non-dimensional parameter α and a modified definition of the Cauchy number are introduced:

$$\alpha = \frac{A}{l}, \quad \mathrm{Ca^s} = \frac{1}{2}\frac{\rho C_D b U_M^2 l^3}{EI}, \tag{2}$$

where $U_M = \omega A$. α is the ratio of the oscillatory flow's amplitude to the structure's length.

For a bunch of multiple blades, we introduce the equivalent thickness and bending stiffness approach. Specifically, for a collection of N blades, the entire assembly is treated as a single entity with an effective thickness of Nd and an effective bending stiffness of NEI, where d and EI are the thickness and bending stiffness of an individual blade, respectively.

We employ an analytical model and the explicit truss-spring numerical model [1] to investigate blade reconfiguration and drag loads. The latter has been validated against experimental results by [2] on the reconfiguration of elastic blades in oscillatory flows (see [1] for detailed methodology).

3 RESULTS

In this section, the experimental results in steady and unsteady flows are presented using non-dimensional parameters. Both experiments encompassed $\beta \in [0.765, 0.993]$, $\mathrm{B} \in [726.1, 2904.6]$, $\lambda \in [5.4, 23.7]$. The steady flow tests spanned $\mathrm{Ca^c} \in [6.28 \times 10^1, 2.08 \times 10^6]$, while the forced oscillation tests covered $\mathrm{Ca^s} \in [1.67 \times 10^3, 1.42 \times 10^5]$ and $\alpha \in [0.77, 2.51]$.

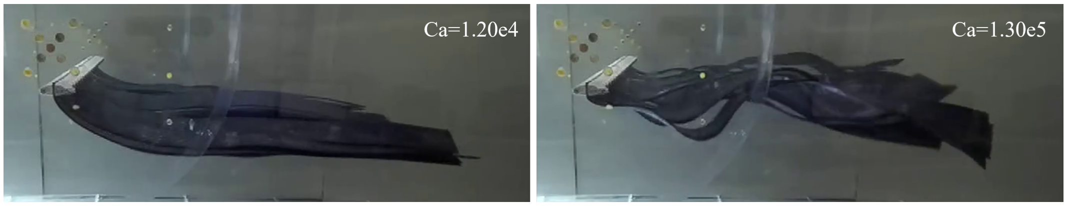

Figure 1: Static reconfiguration at $\mathrm{Ca}^{\mathrm{c}} = 1.20 \times 10^4$ and flutter at $\mathrm{Ca}^{\mathrm{c}} = 1.30 \times 10^5$ in steady flow.

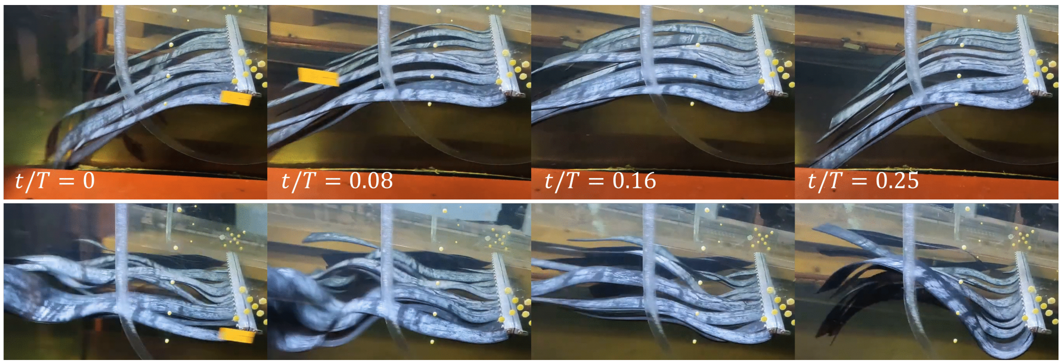

Figure 2: Snapshots of the blades during the second quarter of a cycle ($\pi/2 < \omega t < \pi$). Top row: no flutter, $\mathrm{Ca}^{\mathrm{s}} = 1.58 \times 10^4$, $\alpha = 1.06$; bottom row: flutter, $\mathrm{Ca}^{\mathrm{s}} = 3.56 \times 10^4$, $\alpha = 2.51$.

3.1 Kinematic regimes and bulk drag coefficient

Two distinct kinematic regimes were observed in both experiments: the static regime at low Ca and the flutter regime beyond the critical Ca. Photographs depicting these regimes under steady and unsteady flows are shown in fig. 1 and fig. 2, respectively. The blade kinematics exhibit significant differences between the two regimes.

We calibrate the bulk drag coefficient in steady flows and unsteady flows, respectively, using

$$C^{\mathrm{c}}_{D,\mathrm{bulk}} = \frac{\overline{F_x}}{1/2\rho b l U^2}, \quad C^{\mathrm{s}}_{D,\mathrm{bulk}} = \frac{\overline{F_x U}}{1/2\rho b l \overline{|U|U^2}}. \tag{3}$$

where F_x is the measured horizontal force on the blade mimics. Ca is found to be the primary variable in both scenarios. Although Ca appears in both scenarios, it is defined slightly differently. Since both experiments utilized the same blade mimics and arrangements, a comparison between the two data sets is feasible without additional normalization. We first define the effective flow velocities U_e as the variance of the external flow velocity:

$$U^{\mathrm{c}}_e = U_c, \quad U^{\mathrm{s}}_e = \sqrt{\frac{1}{T}\int_0^T \left[U_M \sin(\omega t)\right]^2 \mathrm{d}t}, \tag{4}$$

for a uniform current and oscillatory flow, respectively. Using these effective flow velocities, we further define the effective Ca, as $\mathrm{Ca}^{\mathrm{c}}_e = \mathrm{Ca}^{\mathrm{c}}$ and $\mathrm{Ca}^{\mathrm{s}}_e = 1/2\mathrm{Ca}^{\mathrm{s}}$. The two data sets of $C_{D,\mathrm{bulk}}$ are plotted against Ca_e in fig. 3.

In both scenarios, $C_{D,\mathrm{bulk}}$ follows similar trends. Prior to flutter, $C_{D,\mathrm{bulk}}$ decreases with increasing Ca at moderate values, with the rate of decrease closely related to B. This trend persists until the onset of flutter, beyond which $C_{D,\mathrm{bulk}}$ ceases to decrease in the flutter regime. While more details will be presented in the workshop, the effects of the non-dimensional parameters on $C_{D,\mathrm{bulk}}$ are summarized in Table 1. It is obvious that flutter significantly influences both the reconfiguration and the drag loads experienced by the flexible blades. Utilizing the effective Ca, we observe that $C_{D,\mathrm{bulk}}$ for side-by-side blades in oscillatory flows closely align with those in a uniform current within the static regime. This congruence between the two datasets permits the application of the well-established analytical models [3] (e.g., the analytical predictions in fig. 3) developed for uniform currents to predict the drag loads

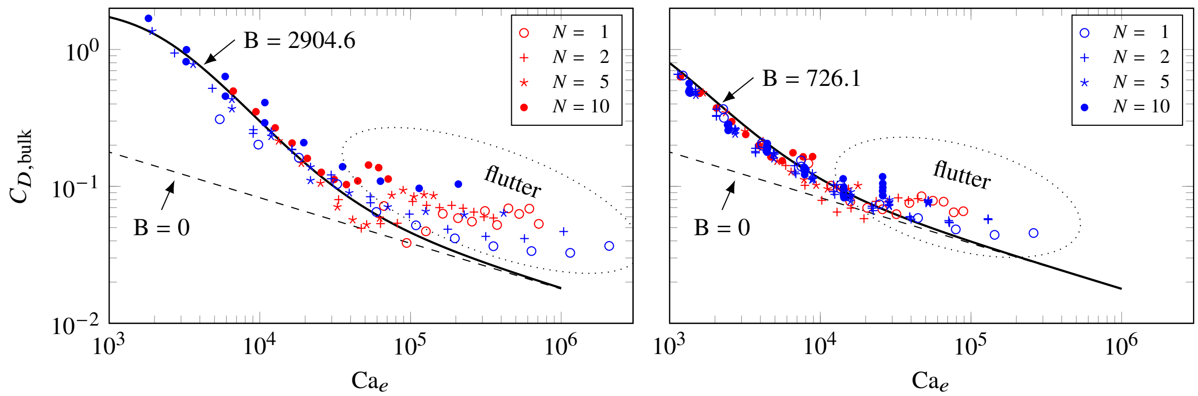

Figure 3: $C_{D,\text{bulk}}$ calibrated from experiments in a uniform current (blue markers) and in oscillatory flows (red markers) for B = 2904.6 (left) and B = 726.1 (right). The black curves and the dashed lines are the analytical prediction with $\lambda \to \infty$.

Table 1: Effects of the common non-dimensional parameters on $C_{D,\text{bulk}}$ and the system stability.

Term	$C_{D,\text{bulk}}$ prior to flutter	System stability	$C_{D,\text{bulk}}$ in flutter regime
β	minimal	stabilizing	negatively correlated
B	positively correlated	stabilizing	depends on β as well
λ	minimal	stabilizing	negatively correlated

on side-by-side blades in oscillatory flows prior to the onset of flutter. On the other hand, in the flutter regime, using the bulk drag coefficient from steady flows underestimates the drag load in oscillatory flows. The latter has industrial relevance to floating seaweed farms exposed to large waves.

3.2 Hydrodynamic load model and system stability

The numerical model uses the same two-dimensional sectional hydrodynamic load model as [2], which consists of two parts, the resistive drag $\boldsymbol{q_d}$ and the reactive force $\boldsymbol{q_{am}}$:

$$\boldsymbol{q_d} = -\frac{1}{2}\rho C_D b|U_n|U_n\boldsymbol{n}, \quad \boldsymbol{q_{am}} = -m_a\left[\frac{\partial(U_n\boldsymbol{n})}{\partial t} - \frac{\partial(U_\tau U_n\boldsymbol{n})}{\partial s} + \frac{1}{2}\frac{\partial(U_n^2\boldsymbol{\tau})}{\partial s}\right], \tag{5}$$

where U_n and U_τ are the normal and tangential components of the relative velocity between the blade and the flow, $m_a = \pi\rho C_M b^2/4$ is the added mass, and s is the arc length along the blade. Using this hydrodynamic load model, our numerical model is able to predict $C_{D,\text{bulk}}$ and the onset of flutter by adjusting the unknown C_M and thus λ, as shown in fig. 4.

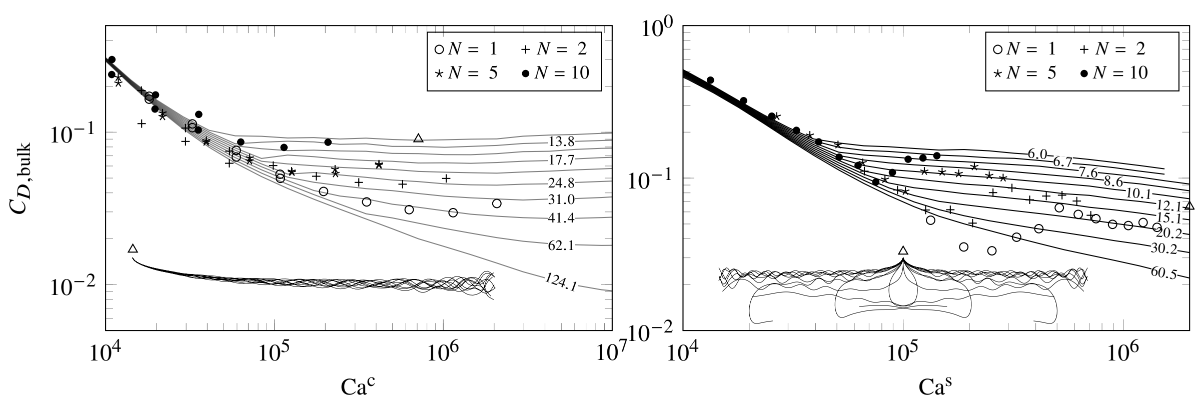

Figure 4: Numerical prediction of $C_{D,\text{bulk}}$ with different λ (lines) and the experimental data for steady flow (left) and unsteady flow (right). The λ values are annotated on the lines. For each scenario, snapshots of the blade trajectory in the flutter regime are also provided at the point marked by triangles.

Table 2: Terms in the reactive force model and their effects on the system stability.

Term	$\partial^2 \boldsymbol{r}/\partial t^2 \cdot \boldsymbol{n}$	$-\partial\theta/\partial t U_\tau$	$-\partial\theta/\partial t U_\tau$	κU_τ^2	$-1/2\kappa U_n^2$
Resulting from	$\partial(U_n \boldsymbol{n})/\partial t$	$\partial(U_n \boldsymbol{n})/\partial t$	$-\partial(U_\tau U_n \boldsymbol{n})/\partial s$	$-\partial(U_\tau U_n \boldsymbol{n})/\partial s$	$1/2\partial(U_n^2 \boldsymbol{\tau})/\partial s$
Corresponds to	$\partial^2\eta/\partial t^2$	$\mathrm{u}\sqrt{\beta}\partial^2\eta/(\partial t \partial s)$	$\mathrm{u}\sqrt{\beta}\partial^2\eta/(\partial t \partial s)$	$\mathrm{u}^2\partial^2\eta/\partial s^2$	0
On system stability	/	stabilizing	stabilizing	destabilizing	none

For an inextensible structure in a steady flow, $\boldsymbol{q_{am}}$ simplifies to

$$\boldsymbol{q_{am}} = -m_a \left[\frac{\partial^2 \boldsymbol{r}}{\partial t^2} \cdot \boldsymbol{n} - 2\frac{\partial \theta}{\partial t} U_\tau + \kappa \left(U_\tau^2 - \frac{1}{2} U_n^2 \right) \right] \boldsymbol{n}. \tag{6}$$

We can investigate the effect of each term in the reactive force model by selectively disabling them in our simulations. By testing different combinations of including or excluding the terms, we list the effects of different terms on the system stability in Table 2. Notably, $\kappa U_\tau^2 = U_\tau^2 \partial\theta/\partial s$ has a destabilizing effect. When this term is excluded, flutter never occurs. The conclusions in Table 2 can also be drawn by comparing the terms in the reactive load model to those in the classic non-dimensional small-amplitude flutter equation for an undamped beam in axial flow:

$$\frac{\partial^2 \eta}{\partial t^2} + 2\mathrm{u}\sqrt{\beta}\frac{\partial^2 \eta}{\partial t \partial s} + \mathrm{u}^2 \frac{\partial^2 \eta}{\partial s^2} + \frac{\partial^4 \eta}{\partial s^4} = 0, \tag{7}$$

where η is the lateral displacement and $\mathrm{u} = \mathrm{Ca}/\lambda$ is the reduced velocity. We apply the Galerkin method to solve Eq. (7). We set $\beta = 0.8$, which falls within the range of our experiments. By excluding $\mathrm{u}^2\partial^2\eta/\partial s^2$, which corresponds to κU_τ^2 in Eq. (6), we find that all modes remain stable regardless of the value of u, as shown in fig. 5 where dimensionless complex frequencies of the four lowest modes are presented. By halving the second term in Eq. (7), equivalent to reducing β to one quarter to its original value, system instability occurs at lower u. Those observations are consistent with the conclusions in Table 2. The traditional Morison's equation, not including the term κU_τ^2, is insufficient to trigger flutter or predict the drag reduction in application of highly compliant structure. More results will be presented in the workshop. This work was supported by Alliance Scholarship at Technical University of Denmark and the Research Council of Norway through SFI BLUES, grant number 309281.

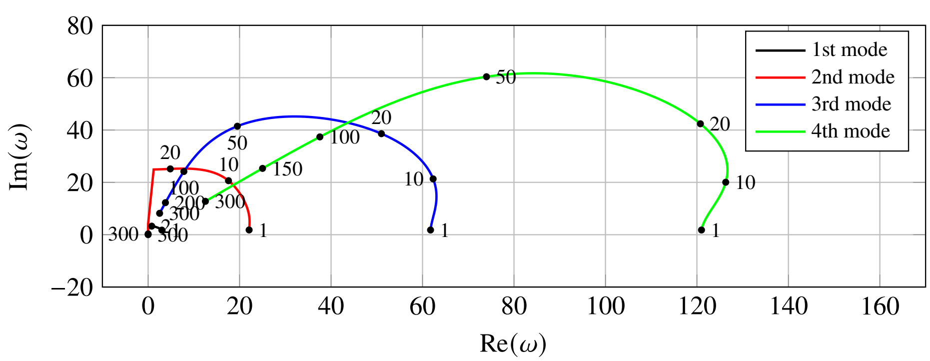

Figure 5: The dimensionless complex frequency of the four lowest modes ($\beta = 0.8$) as a function of the reduced velocity annotated along the curves when $\mathrm{u}^2\partial^2\eta/\partial s^2$ is excluded. $\mathrm{Im}(\omega)$ remains positive, which indicates stability.

REFERENCES

[1] Wei, Z., Shao, Y., Kristiansen, T., and Kristiansen, D. Oct. 2024. *An efficient numerical solver for highly compliant slender structures in waves: Application to marine vegetation. Journal of Fluids and Structures 129*, 104170.

[2] Leclercq, T., and de Langre, E. Jan 2018. *Reconfiguration of elastic blades in oscillatory flow. Journal of Fluid Mechanics 838*, 606–630.

[3] Leclercq, T., Peake, N., and de Langre, E. Jan. 2018. *Does flutter prevent drag reduction by reconfiguration?* Proceedings of the Royal Society A: Mathematical, Physical and Engineering Sciences 474(2209), 20170678.